Two distinct waves of greening in northeastern Canada: summer warming does not tell the whole story

Arthur Bayle, Alexandre Roy, Jean-Pierre Dedieu, Stéphane Boudreau, Philippe Choler, Esther Lévesque

ENVIRONMENTAL RESEARCH
LETTERS

LETTER • OPEN ACCESS

Two distinct waves of greening in northeastern Canada: summer warming does not tell the whole story

To cite this article: Arthur Bayle *et al* 2022 *Environ. Res. Lett.* **17** 064051

ENVIRONMENTAL RESEARCH
LETTERS

LETTER

Two distinct waves of greening in northeastern Canada: summer warming does not tell the whole story

Arthur Bayle[1,*], **Alexandre Roy**[2,3], **Jean-Pierre Dedieu**[2,4], **Stéphane Boudreau**[2,5], **Philippe Choler**[1] and **Esther Lévesque**[2,3]

[1] Université Grenoble Alpes, Université Savoie Mont Blanc, CNRS, LECA, Grenoble, France
[2] Centre d'études nordiques (CEN), 2405, rue de la Terrasse, Quebec City, Québec G1V 0A6, Canada
[3] Département des sciences de l'environnement, Université du Québec à Trois-Rivières, Trois-Rivières, Quebec, Canada
[4] Institute for Geosciences and Environmental Research (IGE), University Grenoble-Alpes/CNRS/IRD/Grenoble-INP, 38058 Grenoble, France
[5] Department de biologie, Université Laval, 1045, avenue de la Médecine, Quebec City, Québec G1V 0A6, Canada
[*] Author to whom any correspondence should be addressed.

E-mail: arthur.bayle.env@gmail.com

Keywords: greening, Landsat, high latitude, vegetation, NDVI

Supplementary material for this article is available online

OPEN ACCESS

RECEIVED
10 March 2022

REVISED
20 May 2022

ACCEPTED FOR PUBLICATION
31 May 2022

PUBLISHED
10 June 2022

Abstract

Arctic vegetation cover has been increasing over the last 40 years, which has been attributed mostly to increases in temperature. Yet, the temporal dimension of this greening remains overlooked as it is often viewed as a monotonic trend. Here, using 11 year long rolling windows on 30 m resolution Landsat data, we examined the temporal variations in greening in north-eastern Canada and its dependence on summer warming. We found two significant and distinct waves of greening, centred around 1996 and 2011, and observed in all land cover types (from boreal forest to arctic tundra). The first wave was more intense and correlated with increasing summer temperature while no such relation was found for the weaker second wave. More specifically, the greening lasted longer at higher elevation during the first wave which translates to a prolonged correlation between greening and summer warming compared to low-altitude vegetation. Our work explored a forsaken complexity of high latitude greening trends and associated drivers and has raised new questions that warrant further research highlighting the importance to include temporal dimension to greening analyses in conjunction with common spatial gradients.

1. Introduction

Global surface air temperatures have increased by roughly 0.12 °C per decade over the past 60 years (Stocker *et al* 2013), with the most rapid warming having occurred in high latitude and mountainous regions (Wang *et al* 2013, 2016, Gobiet *et al* 2014). One of the most noticeable impacts of climate change on high latitude vegetation is the 'greening' of the Arctic and subarctic landscapes (Treharne *et al* 2018, Piao *et al* 2019) which is commonly defined as a multi-decadal increase in remotely-sensed proxies for primary productivity (Myers-Smith *et al* 2020). Despite a global greening trend (Zhu *et al* 2016, Zhang *et al* 2017), periods of relative stability or even 'browning' have also been observed over the last 20 years (De Jong *et al* 2011, Phoenix and Bjerke 2016, Wu *et al* 2020). This spatial and temporal heterogeneity has been attributed in part to a progressive decoupling of the predominant climatic drivers with an apparent weakening of the relationship with temperature (Piao *et al* 2014, Vickers *et al* 2016), while other drivers, such as summer moisture deficit (Sulla-Menashe *et al* 2018) or early snowmelt, appear to be more important (Bokhorst *et al* 2016).

Over the last decades, high latitude vegetation changes have been inferred from optical remote sensing vegetation indices, such as the normalized difference vegetation index (NDVI), a radiometric measurement of horizontal and vertical vegetation cover (Tucker and Sellers 1986, Carlson and Ripley 1997). Most of these studies used time series of NDVI from coarse satellite imagery including the Advanced

Very High Resolution Radiometer (AVHRR) and the Moderate Resolution Imaging Spectroradiometer with spatial resolutions of 1–8 km and 0.25–1 km, respectively (Myers-Smith *et al* 2020). These satellites have shown a widespread but non-uniform greening with sparse browning trends in several regions (Park *et al* 2016). Nonetheless, there are strong discrepancies among AVHRR NDVI data sets (Guay *et al* 2014) and between satellites (Parent and Verbyla 2010, Ju and Masek 2016). For example, while Ju and Masek (2016) reported a fast greening in north-eastern Canada since 1984 using the high-resolution (30 m) Landsat time series, analyses of AVHRR data suggested much slower trends. These inconsistencies highlight the complexity of tackling vegetation dynamics from space.

In fact, beyond remote-sensing related uncertainties (Soudani and Francois 2014), positive changes in NDVI have been linked to changes in species dominance (McManus *et al* 2012, Ropars and Boudreau 2012), increases in plant height or biomass of pre-existing vegetation (Hudson and Henry 2009, Bjorkman *et al* 2018), and/or colonization by vegetation of previously barren land surfaces (Elmendorf *et al* 2012). All these changes appear to be driven mainly by increases in summer temperature (Berner *et al* 2020) and water availability (Arndt *et al* 2019), while fires, insect defoliation (Sulla-Menashe *et al* 2018), or herbivory pressure (Campeau *et al* 2019) can have negative impacts on NDVI trends. As these ecological processes can occur both simultaneously and consecutively on the same area of land, NDVI should exhibit a non-unimodal response.

To date, studies of the complexity of high latitude greening have mostly focused on its spatial variability (Myers-Smith *et al* 2020). In comparison, far less attention has been paid to temporal heterogeneity (Wolkovich *et al* 2014) which is why we need more studies that focus on the temporal variabilities in these ecosystems. Recent studies of the non-linearity and non-stationarity of greening trends have focused on identifying turning points in the time series (Verbesselt *et al* 2010, Jamali *et al* 2015, Yang *et al* 2021). However, these methods can only capture abrupt changes in linear trends but cannot account for more complex, wave-like temporal variations in NDVI time series.

Here, we present a new approach that attempts to diagnose the nonlinear responses of NDVI over the last decades in the George and Koroc rivers watersheds, North-Eastern Canada. These areas cover a large range of latitudes and surface elevations with vegetation coverage spanning from boreal forests (BFs) to arctic shrublands. Our analysis is based on rolling-window regressions, a commonly used time series analysis technique to examine variations in the regression coefficients (Zivot and Wang 2006). With this approach we can investigate temporal variations in trends without *a priori* knowledge regarding the timing of these changes. Furthermore, the results are easy to interpret as the method employs a simple, median-based, linear model commonly used in greening trend studies. We apply this method to a 36 year dataset of Landsat observations and climatic data to answer three questions: (a) Is there a strong temporal heterogeneity in either the greening trend or magnitude during this 36 year period? (b) If yes, what is the spatial structure of this temporal heterogeneity with regard to latitude and altitude gradients and changes in land cover type? (c) What is the relationship between summer warming and greening trends and how has it varied over time and space?

2. Data and sampling design

2.1. Study area

The study area is located in north-eastern Canada and contains the George and Koroc River watersheds, which extend from the Schefferville boreal region in the South to the Ungava Bay arctic region in the North (figure 1). Overall, with increasing latitude the surface elevation also increases from 400 m a.s.l. in the south (55°) to 1000 m a.s.l. in the north-eastern Torngat mountain range at the Quebec-Labrador border (58°–60° N) (figure 1(a)). We divided the land cover types from Leboeuf *et al* (2018) into six categories, namely BF, sub-arctic vegetation (SAV), erect shrub tundra (EST), erect shrub tundra dominated by rocks (ESTRs), prostrate shrub tundra (PST), and prostrate shrub tundra dominated by rocks (PSTRs) (figure 1(b)). The definition and correspondence of each land cover from Leboeuf *et al* (2018) is as follows. BF consists mostly of coniferous forests with understory vegetation dominated by lichens, mosses and ericaceous shrubs (Forêt de résineux', RaL, RcmL, RmD and RmL). SAV corresponds to a mixture of subarctic heathlands, various cover of lichens and shrubs ('Lande subarctique', LS and 'Lande subarctique avec arbustes', LSA). EST consists of a mixture of erect shrubs (30 cm to 1 m), herbs, lichens and mosses, generally dominated by erect shrubs ('Toundra à arbustes dressés', TD). PST consists of tundra with prostrate shrub (<20 cm) with variable cover of lichen, moss or herbaceous species ('Toundra à arbustes prostrés', TP). ESTR and PSTR are variants from EST and PST but dominated by bare outcrops, boulders, stones or mineral soil (TDR and TPR respectively).

2.2. Landsat data and correction workflows

The study area covers 20 path/row numbers (tiles) of the Landsat Worldwide Reference System. We used all available standard Level-1 terrain-corrected orthorectified Landsat surface reflectance images from Collection 1 (geolocation error < 12 m) of the two month period from 1 July to 31 August for the 37 years from 1984 to 2019 (figure 1S (available online at stacks.iop.org/ERL/17/064051/mmedia)), archived

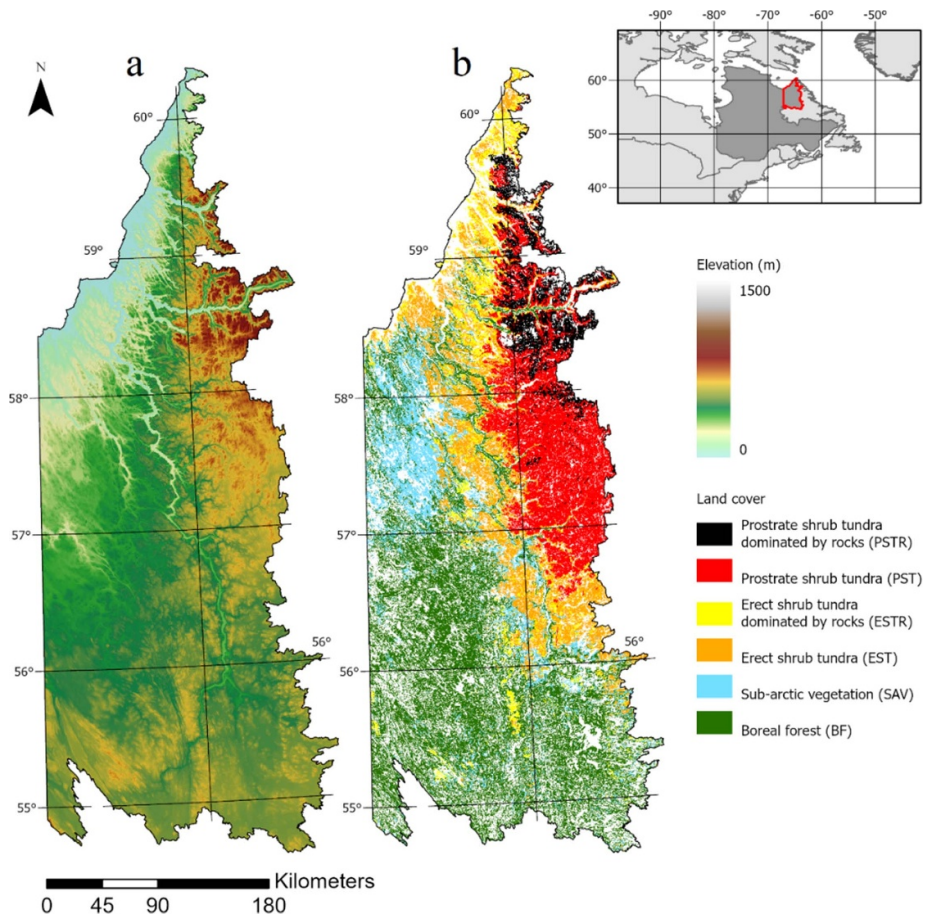

Figure 1. Location of the George and Koroc River basins in Northern Québec, Canada, showing (a) a physical map and (b) the main land cover as obtained from Leboeuf et al (2018), based on Landsat and RapidEye data (Leboeuf and Fournier 2015).

by the Google Earth Engine (Gorelick *et al* 2017) platform as the image collection of United States Geological Survey Landsat 5/7/8 surface reflectance (SR). Images with an average cloud cover >80% were discarded as high cloud cover reduces the number of available ground control points and thus geolocation accuracy. Low-quality observations due to clouds, cloud shadows, cirrus, snow/ice, and scan-line corrector (SLC)-off gaps were identified using the Fmask approach (version 3.3) (Zhu and Woodcock 2012, Zhu *et al* 2015). Using ordinary least squares with the parameters from Roy *et al* (2016a), we converted OLI to ETM+. No correction was applied to TM or ETM+ as SR products from LEDAPS have been shown to be consistent through time, with no differences in the data from before and after the Landsat 7 ETM+ SLC failure in 2003, or between TM and ETM+ (Claverie *et al* 2015). Bidirectional reflectance distribution function (BRDF) effects were corrected using a c-factor approach (Roy *et al* 2016b) based on the RossThick-LiSparse BRDF model (Schaaf *et al* 2002) to account for the 'view angle effect', 'day of year effect', and the 'mean local time drift effect' (Gao *et al* 2014, Nagol *et al* 2015, Qiu *et al* 2021) which all add uncertainties to interannual comparisons of Landsat data (Zhang and Roy 2016, Roy *et al* 2020, Qiu *et al* 2021). Topographic correction was not considered necessary as the slope angles in the study area (quantile 90% = 7.75°) are too small to impact reflectance (Dymond and Shepherd 1999). The NDVI was computed using Normalized BRDF SR in the red and near-infrared spectral bands, retaining pixels with NDVI values >0.1 to assess trends in vegetated surfaces only (Fretwell *et al* 2011, Bayle *et al* 2021). The maximum NDVI (NDVImax) was computed as the annual maximum per pixel from the period 1 June–31 August of each year (Day of year ~152–243). Due to variations in cloud cover, image density, and phenology NDVImax occurred on different dates each year. To prevent errors in NDVImax trend estimation, we discarded those years in which the date of NDVImax differed by more than $\pm 2\sigma$ from the overall mean (figure 2S).

2.3. Climate data

Air temperatures and water conditions for our study area from 1984 to 2019 were obtained from the global monthly 4 km gridded TerraClimate data set available

from the University Corporation for Atmospheric Research (Abatzoglou *et al* 2018) which combines high spatial resolution climatological normal from the WorldClim dataset with coarser, time-varying data from other sources to produce estimates of precipitation, water deficit, and temperature data, among others. From the monthly minimum and maximum temperatures, we computed the summer warmth index (SWI) as the sum of the mean monthly air temperatures exceeding 0 °C during the period from June to August, commonly used as an indicator of cumulative heat load in the Arctic (Bhatt *et al* 2017, Berner *et al* 2018, 2020). The sum of summer precipitation and the sum of summer water deficit as the respective sums of monthly precipitation and water deficit between June and August of each year.

2.4. Sampling design

Our study relies on two distinct samples of pixels both designed to minimize border effects and maximize within-pixel land cover homogeneity. Firstly, we selected pixels corresponding to each medoid of the six land cover classes using the tool 'Feature to Point' from ArcGIS 10.4.1 with 'Inside' option, which yielded 109 447 samples. To reduce spatial dependencies among samples, we removed samples where the nearest neighbour was closer than 300 m (leaving $n = 86\,339$, figure 3S). We also discarded samples for which there were less than 20 years of Landsat records available ($n = 85\,830$) and unvegetated or sparsely vegetated pixels with a mean NDVI (1984–2019) lower than 0.1 to retain vegetated pixels only ($n = 85\,703$). We did not account for human related land cover changes or fire which are both known to be extremely sporadic in our study area. Secondly, to understand the relation between NDVImax trends and climate, we calculated the spatial averages of the NDVI values obtained from the above approach for each 4 km pixel in the TerraClimate data set ($n = 7933$). Elevation and latitude were obtained from the 10 m spatial resolution regional hydro coherent digital elevation model by the Ministry of Energy and Natural Resources of Québec, and Natural Resources Canada (https://mern.gouv.qc.ca/repertoire-geographique/modeles-numeriques-terrain-hydro-coherents-echelle-regionale/), resampled at 30 m and extracted for the first sample set. Following the same procedure as for the NDVI data, we averaged this 30 m resolution elevation and latitude data to each 4 km TerraClimate pixel. Each TerraClimate pixel was assigned one class of land cover based on a majority rule from the first sample set.

3. Methods and statistical analysis

Temporal variability in NDVImax trends was assessed by fitting linear models to the period 1984–2019 using an 11 year rolling windows approach. This approach is similar to rolling averages, except that it uses a median-based linear regression rather than an average to each time period (window). NDVImax trends were computed for window widths ranging from 3 to 17 years and a rolling window width of 11 years was chosen as the best compromise between noise reduction and loss of relevant variability (figure 4S). This yielded 26 subsets for the median years 1989–2014. For example, the trend between 1991 and 2001 will be referred to by its median year and range: 1996 $\pm$ 5. We computed trends only for periods including at least ten years of available NDVImax. The linear model is based on the Theil-Sen single median slope and uses the 'mblm' R package (Komsta 2019). The Theil-Sen estimator of the linear trend is much less sensitive to outliers than a least squares estimator. We used the non-parametric, rank based, Mann-Kendall monotonic test to assess the significance of NDVImax time series trends. Direction, magnitude, and significance of NDVImax trends were analysed for the entire period and for each rolling window to assess the temporal variability.

For further analysis, we focused on the two periods that exhibited the strongest greening trends, henceforth referred as the two 'waves' W1 and W2. Significant ($p < 0.05$) greening trends for W1 and W2 were compared by computing simple Spearman correlations for each land cover type and all samples. Then, to compare both the directions and magnitudes of the W1 and W2 trends, we calculated an index α using $atan2(W2/W1)$ in R based on standardized trends W1 and W2. The index was converted from radians to degrees which yielded angles between $-180°$ and $180°$, thus conserving the sign as opposed to the single-argument arctangent function which cannot distinguish between diametrically opposite directions. We then added $180°$ to α to change its range to $0° < \alpha < 360°$. This angular index allows us to combine the absolute magnitude of the greening trends and the relative difference in greening trend magnitude between W1 and W2 (figure 2). To investigate the spatial structure of the greening trends' temporal variability and to facilitate an easier interpretation, we binned α into six equal-size bins (numbered 1–6 in figure 2) for each land cover type. We further investigated the relation between elevation and the six bins for the PSTR land cover type. We investigated the trends and inter-annual co-variation between SWI and significant greening trends ($p < 0.05$) for each rolling window and land cover type using our second sample set ($n = 7933$, 4 km resolution). Inter-annual co-variation was evaluated through the computation of NDVImax and SWI anomalies which were obtained as the residuals from linear model.

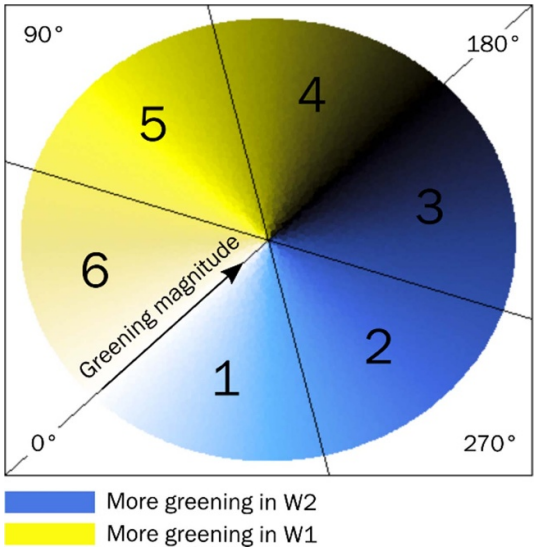

Figure 2. Interpretation of angles of the angular index α for comparing the two greening waves. Angles shaded in yellow correspond to more greening in W1 relative to W2, whereas angles shaded in blue correspond to more greening in W2 relative to W1. Darker colours correspond to more greening. Angles have been divided into six bins to facilitate easier comparisons (see text and figure 5).

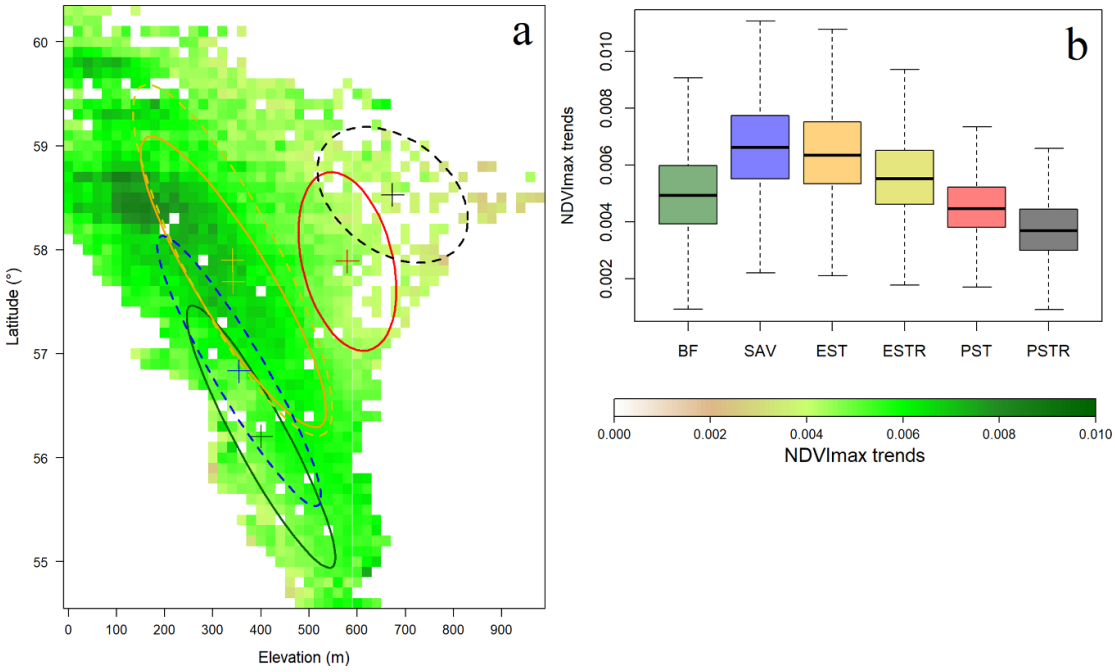

Figure 3. (a) Distribution of NDVImax trends (NDVImax yr^{-1}) along latitudinal and elevational gradients. Ellipses represent 50% confidence intervals for each land cover type. (b) Distribution of NDVImax trends by land cover type. See figure 1 for abbreviations of land cover types.

4. Results

4.1. Spatiotemporal heterogeneity of greening

The emerging linear trend of NDVImax over the 36 year period indicates that over 90% of the pixels showed a significant increase in NDVImax ($p < 0.05$), particularly at latitudes between 57° and 59°N and below elevations of 500 m, which mostly corresponds to SAV and tundra dominated by erect shrub (EST and ESTR). Although greening occurred in all land cover types, BF and tundra dominated by prostrate shrubs (PST and PSTR) showed lower overall increases in NDVImax over time (figure 3). We found a strong temporal variability in both the direction and magnitude of NDVImax trends with two distinct waves of greening separated by a period with near-constant NDVImax values (figure 4). The first wave (W1) occurred between 1991 and 2001 (1996 ± 5) with almost 80% of sample points showing a significant greening ($p < 0.05$) which peaked at 0.016

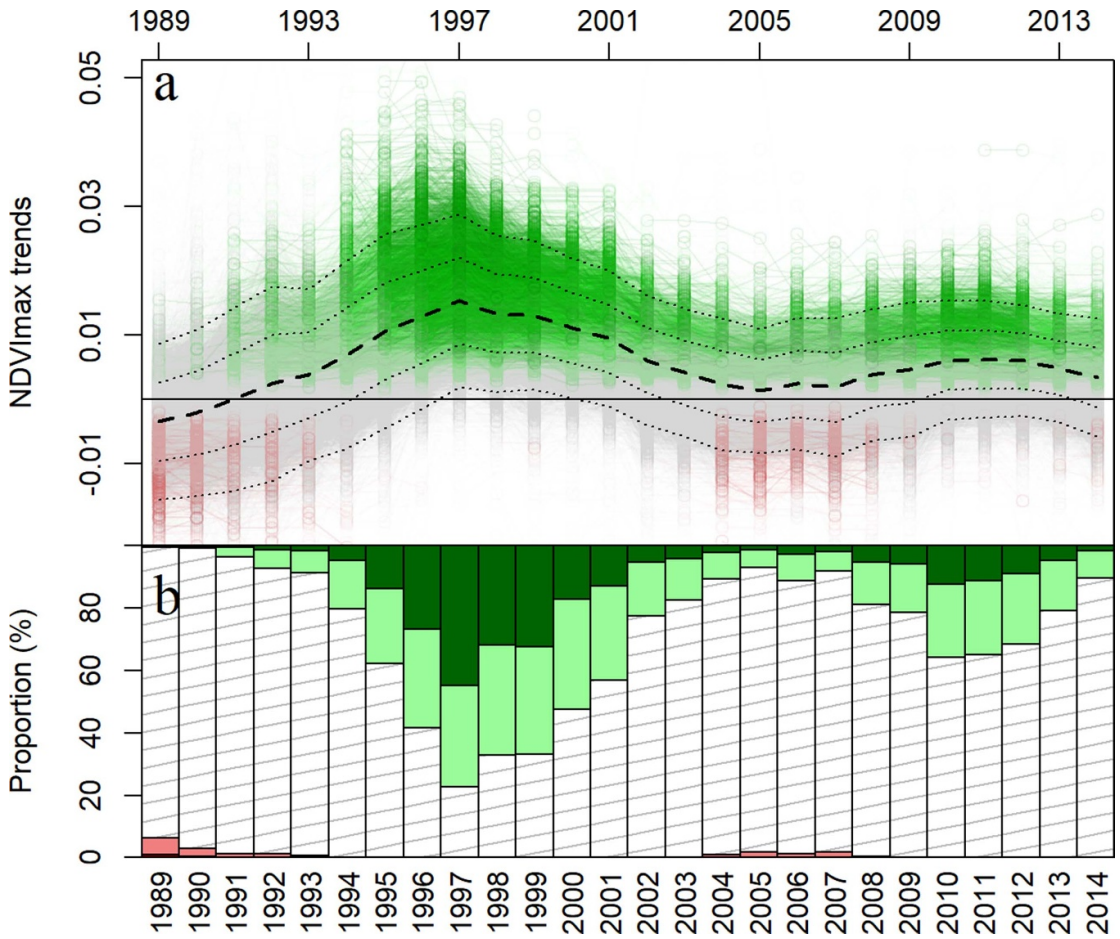

Figure 4. (a) Time series of NDVImax trends showing the mean slope in a median year as a thick, dashed line with standard deviations shown as thin dashed lines (SD and 2SD). Green lines and points represent significant and positive time series ($p < 0.05$), their red equivalents represent significant and negative time series ($p < 0.05$), and grey colour indicates a lack of statistical significance ($p > 0.05$). (b) Time series of the proportion of pixels with positive (dark green: $p < 0.01$; pale green: $p < 0.05$) and negative significant trends (dark red: $p < 0.01$; light coral: $p < 0.05$).

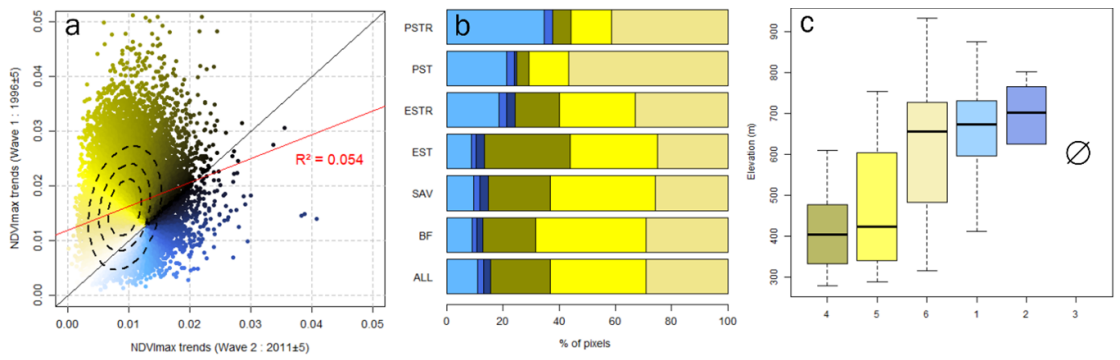

Figure 5. (a) Comparing NDVImax trends for W1 (1996 ± 5) and W2 (2011 ± 5). The red line shows the linear model fit with correlation coefficient R^2. The ellipses, from larger to smaller, represent the 25, 50, and 70% probability contours. The colours corresponds to α as defined in figure 2. (b) Percentage of pixels that fall into the six different bins of α (see figure 2) for each land cover type. (c) Distribution of land surface elevation for the different α bins of the PSTR land cover type. Refer to figure 1 for the abbreviations of land cover types.

NDVImax yr^{-1}. The second wave (W2) occurred in 2011 ± 5 but was not as strong, with significant greening observed for only 30% of sample points at a lower average rate of 0.0075 NDVImax/year. In fact, at 83% of sample locations the greening was weaker in W2 compared to W1 (figure 5(b)), with only some higher elevation locations experiencing stronger greening during W2 (around 25% for PSTR) (figure 5(c)). There was no correlation between the greening rates measured in W1 and W2 at each sample point (Spearman's coefficient, $\rho = 0.054$) (figure 5(a)). Outside W1 and W2, only the PSTR land cover appears to

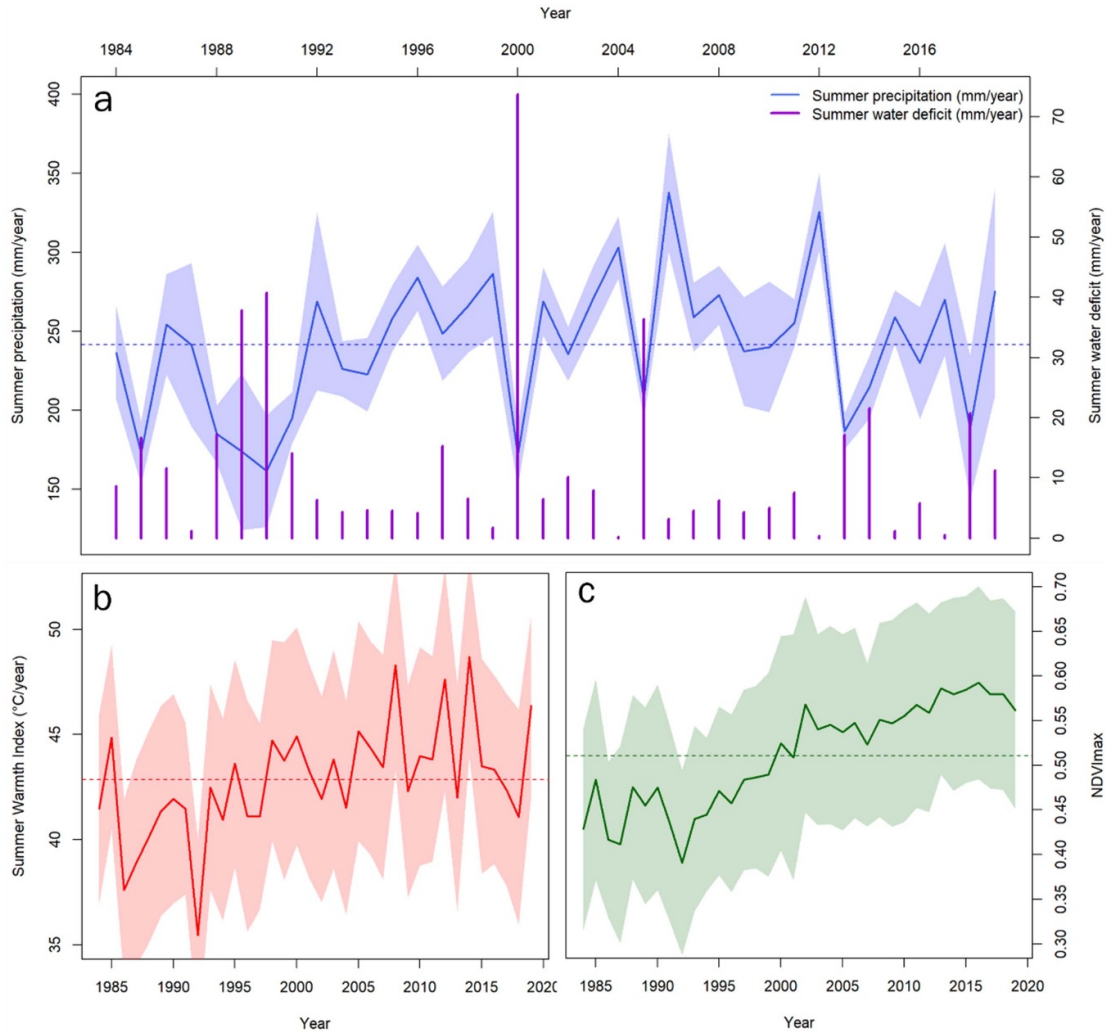

Figure 6. (a) Time series of summer precipitation and summer water deficit from 1984 to 2019 based on the TerraClimate dataset. (b) Time series of Summer Warmth Index from 1984 to 2019. (c) Time series of Landsat-based NDVImax from 1984 to 2019. The dashed horizontal lines in each panel represent the averages while envelopes show one standard deviation.

display some greening (figure 5S). Interestingly, some pixels also displayed significant browning trends over the study period (figure 4(b)).

4.2. Effect of summer warming on greening

Overall, summer precipitation did not exhibit significant trends over the 36 years although we did find some years with significant water deficits (1989, 1990, 2000, 2005 and 2012) (figure 6(a)). On average, high precipitation was observed during the 1990s and from 2006 to 2012. Time series of SWI showed significant warming during the 1990s marked by a strong negative anomaly in 1992, caused by the eruption of Mount Pinatubo (Lucht *et al* 2002). Since 2000, summer temperatures have varied and even decreased between 2005 and 2019, yet this period is marked by four of the warmest years since 1984 (2008, 2012, 2014, and 2019) (figure 6(b)). The two greening waves showed differing correlations with SWI (figure 7). While W1 was marked by a strong correlation between NDVImax and SWI ($\rho = 0.57 \pm 0.17$), no significant correlation was found for W2 ($\rho = -0.06 \pm 0.25$) (figure 7(a)). The same computation using NDVI and SWI anomalies showed similar results with moderate correlations for W1 ($\rho = 0.3 \pm 0.22$) and no correlation for W2 (figure 7(b)). The distribution of correlations shows that almost all pixels exhibiting greening were correlated to summer warming in W1 (figure 7(c)). At the end of W1, a slight negative correlation between NDVImax and SWI anomalies was observed (figure 7(d)). These correlations were found for all land cover classes except arctic tundra (PST and PSTR). The positive correlation between NDVImax and SWI appears to last longer after W1 for PST and PSTR (figure 8(a)). Furthermore, we found stronger correlations between NDVImax and SWI anomalies for PSTR at the end of W1 (figure 8(b)).

5. Discussion

Our detailed study of NDVI trends in northeastern Canada has provided significant insights to deepen our knowledge of the greening of Arctic and subarctic landscapes. First, while we showed that the

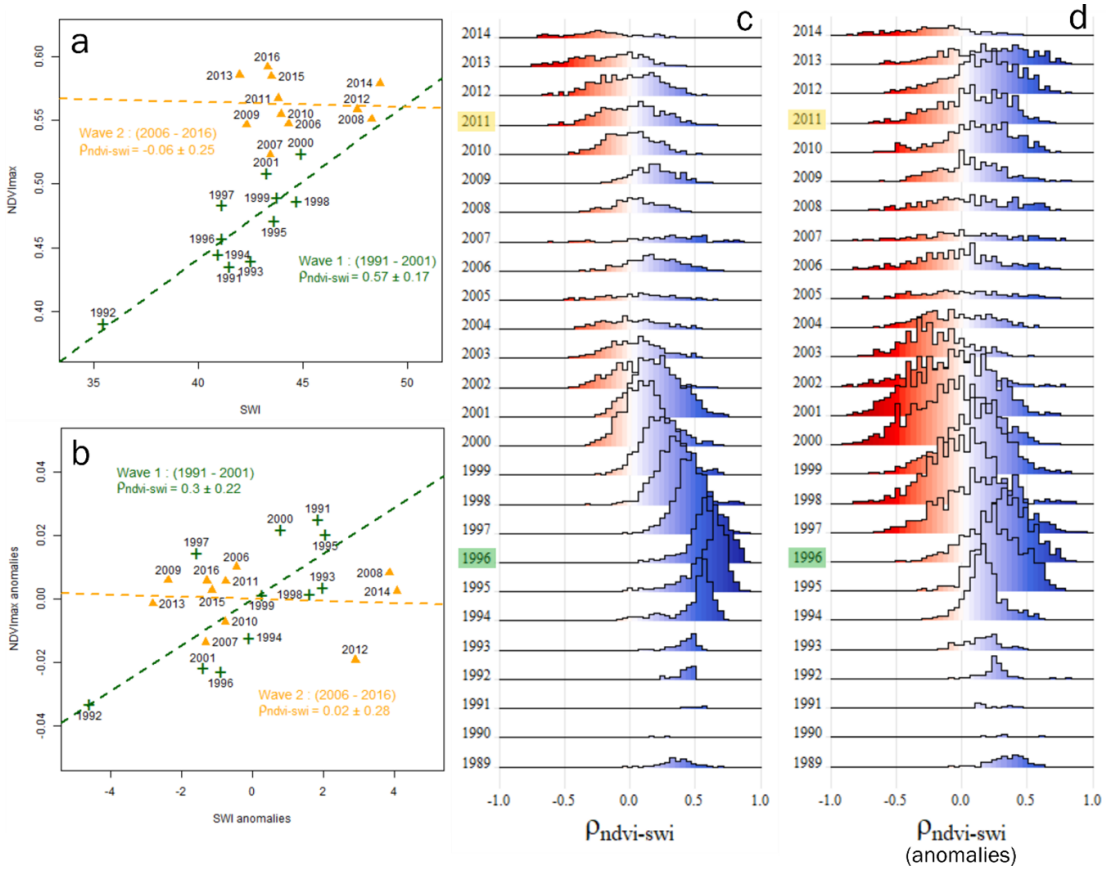

Figure 7. Correlation between (a) NDVImax and SWI, and (b) anomalies of NDVImax and SWI for W1 (green) and W2 (yellow). Spearman's correlation coefficients and corresponding standard deviation are shown for each wave. Distributions of Spearman's correlation coefficients for each rolling window for (c) NDVImax and SWI and (d) anomalies of NDVImax and of SWI. For (c) and (d), each year represents the median year of the rolling window.

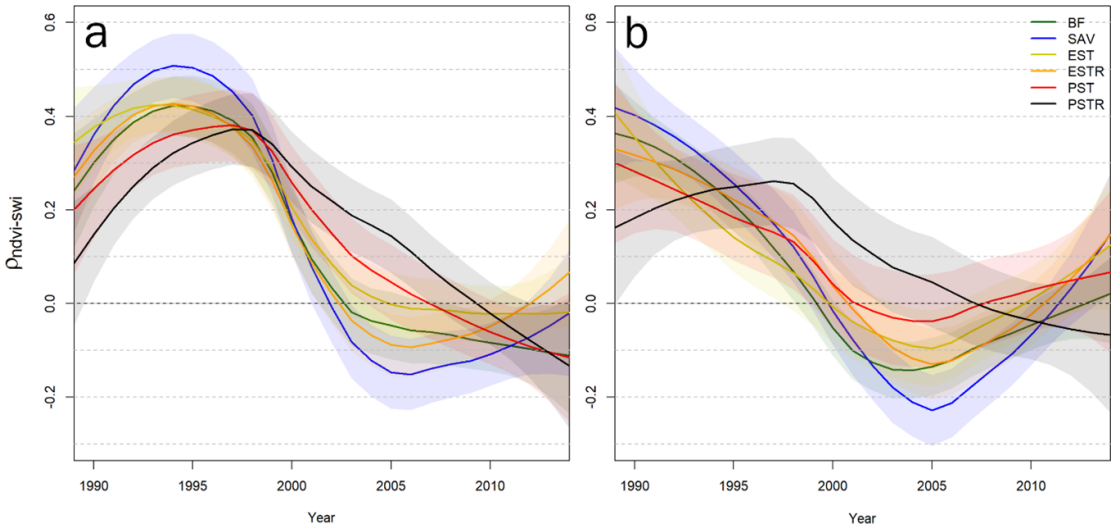

Figure 8. Distribution of Spearman's correlation coefficients for (a) NDVImax and SWI, and (b) anomalies of NDVImax and of SWI for each rolling window and land cover type. Time series were smoothed using LOESS regression. The coloured band represent the 97.5% confidence intervals for each land cover type. Refer to figure 1 for the abbreviations of land cover types.

study region experienced a strong greening trend over the 1984–2019 period, this trend is characterized by an important temporal heterogeneity as two distinct greening waves were observed during that period (figure 4). Second, all land cover types—i.e. from BF to arctic PST—displayed significant greening over that period although the two greening waves differed in intensity as greening was more intense in the first wave compared to the second one, but at different proportion depending on elevation (figure 5). Third,

we found no consistent effect of summer warming on greening: while we observed strong relationship between NDVI and SWI during the first wave, there was no correlation during the second (figure 7).

Our study investigated the temporal heterogeneity of NDVI changes across a vast and diverse landscape. As our analysis relied on a unique high-resolution remote sensing approach for a wide range of vegetation types and topography, it inevitably calls into question the meaning of NDVI variations over time and the scale at which we observed it. In general, increases in NDVI can be attributed to changes in biomass production of established plants and/or to the establishment of newcomers with unknown consequences on NDVI values. Hence, an increase in NDVI of 0.1 over a particular time period but for two different vegetation types would not have the same ecological significance, illustrating the difficulty of using satellite-based proxies of vegetation cover to make statements regarding local ecosystems. In addition, the unavailability of *in situ* observation limits our ability to assign specific ecological processes to NDVImax trajectories (McManus *et al* 2012, Bonney *et al* 2018, Sulla-Menashe *et al* 2018). Thus, we rely on our reflectance correction workflow and the near absence of human impacts on our study area (section 2.2) to assume that significant changes in NDVI over time result from changes in vegetation cover at a pixel scale. Furthermore, by using high-resolution Landsat imagery, we minimize the probability of opposing trends occurring within a pixel as these small pixels represent more homogeneous vegetation types and topographies. This is key when studying vegetation dynamics across latitudes and altitudes as this necessarily involves complex ecotones and heterogeneous landscapes (Ropars and Boudreau 2012). Finally, our sampling strategy based on distance thresholding and land cover medoid selection, was designed to minimize these issues by limiting spatial autocorrelations. Overall, we are therefore confident that our approach is suitable to reliably identify real changes in ground vegetation.

Widespread greening has been reported in many cold, seasonally snow-covered ecosystems (Zhu *et al* 2016, Anderson *et al* 2020, Berner *et al* 2020, Choler *et al* 2021) as a response to the more pronounced warming they experienced over the last few decades compared to lower latitude and altitude ecosystems (Pepin *et al* 2015, Palazzi *et al* 2019). In fact, northeastern Canada has been identified as a greening hotspot by Ju and Masek (2016) and Berner *et al* (2020) based on 1984–2012 Landsat time series data. Our results do corroborate their findings as more than 90% of our study region exhibited significant greening between 1984 and 2019. This homogenous greening in an area that harbours rather diverse vegetation zones and topographical gradients that generate strong environmental gradients over short distances is astounding, considering that greening occurred only on about 40% of the terrestrial land area in the Arctic (Berner *et al* 2020). Such results are likely related to the specific location of our study area, at the transition zone from forest/tundra to the Low Arctic, which is very responsive to warmer air temperatures (Epstein *et al* 2004, Walker *et al* 2006, Lantz *et al* 2010). In this particular region, as well as in other parts of Nunavik, the observed strong positive greening trend is believed to be closely associated to the expansion of *Betula glandulosa* Michx., the main 'species' involved in landscape-level shrubification (Ropars and Boudreau 2012, Tremblay *et al* 2012). Indeed, this species' radial growth has increased sharply in the 1990s (Ropars *et al* 2015) in response to warmer temperatures in this region (Bhiry *et al* 2011). The responsiveness of *B. glandulosa* to climate change could be due to a greater morphological plasticity, as shown for closely related species of the *Betula* genus (Shaver and Cutler 1979, Bret-Harte *et al* 2001).

We were able to demonstrate that the greening observed in our study region between 1984 and 2019 (figure 4) occurred in two distinct and relatively short greening waves lasting from 1991 to 2001 (W1) and 2006–2016 (W2). Historically, temporal patterns of NDVI variation have often been assessed by comparing two overlapping periods (Jeong *et al* 2012, Bhatt *et al* 2013, 2017, Berner *et al* 2020). Such studies found a systematic slowing in greening trends over the last 20 years in comparison to the 1990s. Similarly, since greening in W1 was stronger than in W2 this would also suggest a slowing of the observed greening trends (figure 5(a)), except at high altitudes where greening was stronger in W2 (figures 5(b) and (c)). Such a consistent pattern across most land covers suggests that plant communities respond to a common large-scale driver (figure 5S), likely warmer temperatures (figure 6(b)).

We explored the relation between NDVImax and summer temperature increase through two approaches. Our analysis showed a strong relation between NDVImax and SWI for W1 but not for W2, suggesting that large-scale changes in vegetation cover was triggered by warmer temperatures only in W1 (figures 7(a) and (c)). Comparatively, the analysis of inter-annual covariation (anomalies) between NDVImax and SWI revealed a moderate relation in W1 and no relation in W2 (figures 7(b) and (d)). The negative relation between anomalies of NDVImax and SWI toward the end of W1 corresponds to the inclusion of years characterized by extreme water deficit (2000 and 2005) in the 11 year rolling window, suggesting that drought stress could be the limiting factor that ended the first greening wave. The importance of drought on NDVI was indirectly proposed by Ropars *et al* (2015) based on growth ring data in western Nunavik. Indeed, they demonstrated that while *B. glandulosa* radial growth from 1986 to 2002 explained between 71% and 80% of the NDVI

data variance, the reduced growth between 2000 and 2009 was likely due to negative water balance. In our study, the drought hypothesis is also consistent with the specific response of high-altitude land cover to summer warming (figure 8). As the evapotranspiration demand is likely lower for high-altitude ecosystems with a reduced vascular plant cover, years of drought should have a smaller impact on their primary productivity (Corona-Lozada *et al* 2019). In fact, land covers dominated by prostrated shrubs (PST and PSTR) tend to exhibit a more diffuse W1 than other low-altitude land cover types (figure 5S) which translates into a prolonged positive relation between NDVImax and SWI (figure 8(a)). Furthermore, there is a significant shift in time in the correlation between anomalies of NDVImax and SWI for PSTR despite the important water deficit observed throughout this period (figure 8(b)). For W2, no difference was found in the relationship between summer temperature and NDVImax among land covers. Interestingly, W2 was marked by three years of extreme temperatures (figure 6(b)) which did not result in water deficits as precipitations remained high (figure 6(a)). As heat waves accompanied by high precipitation are favourable to alpine vegetation growth (Corona-Lozada *et al* 2019), it is plausible that temperature remained the main driver of greening but through recurrent extreme heat events instead of long-term trends (Simpkins 2017). Another explanation could be that the second period of greening is the result of the warming observed in the 1990s, as temperatures remained stable between W1 and W2, but with a delay due to water balance deficits in the 2000s that prevented vegetation from fully benefiting from the initial warming. Finally, we did not analyse changes in herbivory pressure over time, though it has been shown that herbivores can alter tundra response to warming (Post and Forchhammer 2008, Campeau *et al* 2019). This might be of importance since the George River caribou herd (*Rangifer tarandus* L.) was abundant in our study region up to the 1990s, before declining progressively until the 2010s. These limitations should be considered for further research.

6. Conclusion

We demonstrated a strong temporal heterogeneity in the greening pattern along a large watershed in northeastern Canada with two distinct greening waves (centred around 1996 and 2011) found during a 36 year period from 1984 to 2019. NDVI increased in all land cover types, from BF to arctic PST, strongly correlated with increased summer temperatures during the first wave but uncorrelated during the second one. We also showed that the first greening wave and its relation to summer warming lasted for a longer time in high-altitude vegetation. Our work explores a forsaken complexity of high latitude greening and has raised new questions that warrant further research highlighting the importance to include the temporal dimension. We emphasize that in order to disentangle the complexity of arctic greening, the temporal domain should be accounted for in conjunction with well-studied spatial gradients which result in the consideration of both forcings and ecological responses as non-stationary (Wolkovich *et al* 2014).

Data availability statement

The data that support the findings of this study are available upon reasonable request from the authors.

Acknowledgments

This research was developed in collaboration with the community of Kangiqsualujjuaq and supported by the Centre d'études Nordiques (CEN). Financial support was provided by OHMi-Nunavik—LabEx DRIIHM, French program 'Investissements d'Avenir' (ANR-11-LABX0010) managed by the French National Research Agency (ANR), Polar Knowledge Canada, ArcticNet (Network of Centres of Excellence of Canada), Crown-Indigenous Relations and Northern Affairs Canada (Indigenous Community-Based Climate Monitoring Program), NSERC-discovery grant (Lévesque). Authors acknowledge the support of the Community of Kangiqsualujjuaq to this project, especially for during the Imalirijiit field camp 2018 that facilitated access to field sites that stimulated the current analysis. Thank you to José Gérin-Lajoie, Xavier Dallaire and Geneviève Dubois for assistance in the field. We also thank Claude Morneau, Martin Simard, Hugues Dorion and José Gérin-Lajoie for support to different aspects of the project. Editorial assistance, in the form of language editing and correction, was provided by XpertScientific Editing and Consulting Services. Finally, anonymous evaluators contributed to improve the manuscript.

ORCID iD

Arthur Bayle https://orcid.org/0000-0002-3442-0789

References

Abatzoglou J T, Dobrowski S Z, Parks S A and Hegewisch K C 2018 TerraClimate, a high-resolution global dataset of monthly climate and climatic water balance from 1958–2015 *Sci. Data* **5** 170191

Anderson K, Fawcett D, Cugulliere A, Benford S, Jones D and Leng R 2020 Vegetation expansion in the subnival Hindu Kush Himalaya *Glob. Change Biol.* **26** 1608–25

Arndt K A, Santos M J, Ustin S, Davidson S J, Stow D, Oechel W C, Tran T T P, Graybill B and Zona D 2019 Arctic greening associated with lengthening growing seasons in Northern Alaska *Environ. Res. Lett.* **14** 125018

Bayle A, Roussel E, Carlson B Z, Vautier F, Brossard C, Fovet E, De Bouchard D'aubeterre G and Corenblit D 2021 Sensitivity of

Landsat NDVI to subpixel vegetation and topographic components in glacier forefields: assessment from high-resolution multispectral UAV imagery *Proc. SPIE* **15** 044508

Berner L T *et al* 2020 Summer warming explains widespread but not uniform greening in the Arctic tundra biome *Nat. Commun.* **11** 4621

Berner L T, Jantz P, Tape K D and Goetz S J 2018 Tundra plant above-ground biomass and shrub dominance mapped across the North Slope of Alaska *Environ. Res. Lett.* **13** 035002

Bhatt U S *et al* 2017 Changing seasonality of panarctic tundra vegetation in relationship to climatic variables *Environ. Res. Lett.* **12** 055003

Bhatt U, Walker D, Raynolds M, Bieniek P, Epstein H, Comiso J, Pinzon J, Tucker C and Polyakov I 2013 Recent declines in warming and vegetation greening trends over pan-Arctic tundra *Remote Sens.* **5** 4229–54

Bhiry N *et al* 2011 Environmental change in the Great Whale River region, Hudson Bay: five decades of multidisciplinary research by Centre d'études nordiques (CEN) *Ecoscience* **18** 182–203

Bjorkman A D *et al* 2018 Plant functional trait change across a warming tundra biome *Nature* **562** 57–62

Bokhorst S *et al* 2016 Changing Arctic snow cover: a review of recent developments and assessment of future needs for observations, modelling, and impacts *Ambio* **45** 516–37

Bonney M T, Danby R K and Treitz P M 2018 Landscape variability of vegetation change across the forest to tundra transition of central Canada *Remote Sens. Environ.* **217** 18–29

Bret-Harte M S, Shaver G R, Zoerner J P, Johnstone J F, Wagner J L, Chavez A S, Gunkelman R F IV, Lippert S C and Laundre J A 2001 Developmental plasticity allowsbetula nanato dominate tundra subjected to an altered environment *Ecology* **82** 18–32

Campeau A B, Rickbeil G J M, Coops N C and Côté S D 2019 Long-term changes in the primary productivity of migratory caribou (*Rangifer tarandus*) calving grounds and summer pasture on the Quebec-Labrador Peninsula (Northeastern Canada): the mixed influences of climate change and caribou herbivory *Polar Biol.* **42** 1005–23

Carlson T N and Ripley D A 1997 On the relation between NDVI, fractional vegetation cover, and leaf area index *Remote Sens. Environ.* **62** 241–52

Choler P, Bayle A, Carlson B Z, Randin C, Filippa G and Cremonese E 2021 The tempo of greening in the European Alps: spatial variations on a common theme *Glob. Change Biol.* **27** 5614–28

Claverie M, Vermote E F, Franch B and Masek J G 2015 Evaluation of the Landsat-5 TM and Landsat-7 ETM+ surface reflectance products *Remote Sens. Environ.* **169** 390–403

Corona-Lozada M C, Morin S and Choler P 2019 Drought offsets the positive effect of summer heat waves on the canopy greenness of mountain grasslands *Agric. For. Meteorol.* **276–277** 107617

De Jong R, De Bruin S, De Wit A, Schaepman M E and Dent D L 2011 Analysis of monotonic greening and browning trends from global NDVI time-series *Remote Sens. Environ.* **115** 692–702

Dymond J R and Shepherd J D 1999 Correction of the topographic effect in remote sensing *IEEE Trans. Geosci. Remote Sens.* **37** 2618–9

Elmendorf S C *et al* 2012 Global assessment of experimental climate warming on tundra vegetation: heterogeneity over space and time *Ecol. Lett.* **15** 164–75

Epstein H E, Beringer J, Gould W A, Lloyd A H, Thompson C D, Chapin F S, Michaelson G J, Ping C L, Rupp T S and Walker D A 2004 The nature of spatial transitions in the Arctic *J. Biogeogr.* **31** 1917–33

Fretwell P T, Convey P, Fleming A H, Peat H J and Hughes K A 2011 Detecting and mapping vegetation distribution on the Antarctic Peninsula from remote sensing data *Polar Biol.* **34** 273–81

Gao F, He T, Masek J G, Shuai Y, Schaaf C B and Wang Z 2014 Angular effects and correction for medium resolution sensors to support crop monitoring *IEEE J. Sel. Top. Appl. Earth Obs. Remote Sens.* **7** 4480–9

Gobiet A, Kotlarski S, Beniston M, Heinrich G, Rajczak J and Stoffel M 2014 21st century climate change in the European Alps—a review *Sci. Total Environ.* **493** 1138–51

Gorelick N, Hancher M, Dixon M, Ilyushchenko S, Thau D and Moore R 2017 Google Earth Engine: planetary-scale geospatial analysis for everyone *Remote Sens. Environ.* **202** 18–27

Guay K C, Beck P S A, Berner L T, Goetz S J, Baccini A and Buermann W 2014 Vegetation productivity patterns at high northern latitudes: a multi-sensor satellite data assessment *Glob. Change Biol.* **20** 3147–58

Hudson J M and Henry G H 2009 Increased plant biomass in a High Arctic heath community from 1981 to 2008 *Ecology* **90** 2657–63

Jamali S, Jönsson P, Eklundh L, Ardö J and Seaquist J 2015 Detecting changes in vegetation trends using time series segmentation *Remote Sens. Environ.* **156** 182–95

Jeong S-J, Ho C-H, Kim B-M, Feng S and Medvigy D 2012 Non-linear response of vegetation to coherent warming over northern high latitudes *Remote Sens. Lett.* **4** 123–30

Ju J and Masek J G 2016 The vegetation greenness trend in Canada and US Alaska from 1984–2012 Landsat data *Remote Sens. Environ.* **176** 1–16

Komsta L 2019 *mblm: Median-Based Linear Models* R package version 0.12.1

Lantz T C, Gergel S E and Kokelj S V 2010 Spatial heterogeneity in the shrub tundra ecotone in the Mackenzie Delta region, Northwest Territories: implications for Arctic environmental change *Ecosystems* **13** 194–204

Leboeuf A and Fournier R A 2015 A multisensor multiresolution method for mapping vegetation status, surficial deposits, and historical fires over very large areas in northern boreal forests of Quebec, Canada *IEEE J. Sel. Top. Appl. Earth Obs. Remote Sens.* **8** 5199–211

Leboeuf A, Morneau C, Robitaille A, Dufour E and Grondin P 2018 Ecological mapping of the vegetation of Northern Québec (Ministère des Ressources naturelles et de la Faune du Québec, Direction des inventaires forestiers)

Lucht W, Prentice I C, Myneni R B, Sitch S, Friedlingstein P, Cramer W, Bousquet P, Buermann W and Smith B 2002 Climatic control of the high-latitude vegetation greening trend and Pinatubo effect *Science* **296** 1687–9

McManus K M, Morton D C, Masek J G, Wang D, Sexton J O, Nagol J R, Ropars P and Boudreau S 2012 Satellite-based evidence for shrub and graminoid tundra expansion in northern Quebec from 1986 to 2010 *Glob. Change Biol.* **18** 2313–23

Myers-Smith I H *et al* 2020 Complexity revealed in the greening of the Arctic *Nat. Clim. Change* **10** 106–17

Nagol J R, Sexton J O, Kim D-H, Anand A, Morton D, Vermote E and Townshend J R 2015 Bidirectional effects in Landsat reflectance estimates: is there a problem to solve? *ISPRS J. Photogramm. Remote Sens.* **103** 129–35

Palazzi E, Mortarini L, Terzago S and Von Hardenberg J 2019 Elevation-dependent warming in global climate model simulations at high spatial resolution *Clim. Dyn.* **52** 2685–702

Parent M B and Verbyla D 2010 The browning of Alaska's boreal forest *Remote Sens.* **2** 2729–47

Park T, Ganguly S, Tømmervik H, Euskirchen E S, Høgda K-A, Karlsen S R, Brovkin V, Nemani R R and Myneni R B 2016 Changes in growing season duration and productivity of northern vegetation inferred from long-term remote sensing data *Environ. Res. Lett.* **11** 084001

Pepin N *et al* 2015 Elevation-dependent warming in mountain regions of the world *Nat. Clim. Change* **5** 424–30

Phoenix G K and Bjerke J W 2016 Arctic browning: extreme events and trends reversing arctic greening *Glob. Change Biol.* **22** 2960–2
Piao S *et al* 2014 Evidence for a weakening relationship between interannual temperature variability and northern vegetation activity *Nat. Commun.* **5** 5018
Piao S *et al* 2019 Characteristics, drivers and feedbacks of global greening *Nat. Rev. Earth Environ.* **1** 14–27
Post E and Forchhammer M C 2008 Climate change reduces reproductive success of an Arctic herbivore through trophic mismatch *Phil. Trans. R. Soc.* B **363** 2369–75
Qiu S, Zhu Z, Shang R and Crawford C J 2021 Can Landsat 7 preserve its science capability with a drifting orbit? *Sci. Remote Sens.* **4** 100026
Ropars P and Boudreau S 2012 Shrub expansion at the forest–tundra ecotone: spatial heterogeneity linked to local topography *Environ. Res. Lett.* **7** 015501
Ropars P, Lévesque E and Boudreau S 2015 Shrub densification heterogeneity in subarctic regions: the relative influence of historical and topographic variables *Ecoscience* **22** 83–95
Roy D P, Kovalskyy V, Zhang H K, Vermote E F, Yan L, Kumar S S and Egorov A 2016a Characterization of Landsat-7 to Landsat-8 reflective wavelength and normalized difference vegetation index continuity *Remote Sens. Environ.* **185** 57–70
Roy D P, Li Z, Zhang H K and Huang H 2020 A conterminous United States analysis of the impact of Landsat 5 orbit drift on the temporal consistency of Landsat 5 Thematic Mapper data *Remote Sens. Environ.* **240** 111701
Roy D P, Zhang H K, Ju J, Gomez-Dans J L, Lewis P E, Schaaf C B, Sun Q, Li J, Huang H and Kovalskyy V 2016b A general method to normalize Landsat reflectance data to nadir BRDF adjusted reflectance *Remote Sens. Environ.* **176** 255–71
Schaaf C B *et al* 2002 First operational BRDF, albedo nadir reflectance products from MODIS *Remote Sens. Environ.* **83** 135–48
Shaver G R and Cutler J C 1979 The vertical distribution of live vascular phytomass in cottongrass tussock tundra *Arct. Alp. Res.* **11** 335
Simpkins G 2017 Extreme Arctic heat *Nat. Clim. Change* **7** 95
Soudani K and Francois C 2014 Remote sensing: a green illusion *Nature* **506** 165–6
Stocker T F *et al* 2013 Climate change 2013: the physical science basis *Intergovernmental Panel on Climate Change, Working Group I Contribution to the IPCC Fifth Assessment Report (AR5)* (New York: Cambridge University Press)
Sulla-Menashe D, Woodcock C E and Friedl M A 2018 Canadian boreal forest greening and browning trends: an analysis of biogeographic patterns and the relative roles of disturbance versus climate drivers *Environ. Res. Lett.* **13** 014007
Treharne R, Bjerke J W, Tommervik H, Stendardi L and Phoenix G K 2018 Arctic browning: impacts of extreme climatic events on heathland ecosystem CO_2 fluxes *Glob. Change Biol.* **25** 489–503
Tremblay B, Lévesque E and Boudreau S 2012 Recent expansion of erect shrubs in the Low Arctic: evidence from Eastern Nunavik *Environ. Res. Lett.* **7** 035501
Tucker C J and Sellers P J 1986 Satellite remote sensing of primary production *Int. J. Remote Sens.* **7** 1395–416
Verbesselt J, Hyndman R, Newnham G and Culvenor D 2010 Detecting trend and seasonal changes in satellite image time series *Remote Sens. Environ.* **114** 106–15
Vickers H, Høgda K A, Solbø S, Karlsen S R, Tømmervik H, Aanes R and Hansen B B 2016 Changes in greening in the High Arctic: insights from a 30 year AVHRR max NDVI dataset for Svalbard *Environ. Res. Lett.* **11** 105004
Walker M D *et al* 2006 Plant community responses to experimental warming across the tundra biome *Proc. Natl Acad. Sci. USA* **103** 1342–6
Wang Q, Fan X and Wang M 2013 Recent warming amplification over high elevation regions across the globe *Clim. Dyn.* **43** 87–101
Wang Q, Fan X and Wang M 2016 Evidence of high-elevation amplification versus Arctic amplification *Sci. Rep.* **6** 19219
Wolkovich E M, Cook B I, McLauchlan K K, Davies T J and Courchamp F 2014 Temporal ecology in the Anthropocene *Ecol. Lett.* **17** 1365–79
Wu W, Sun X, Epstein H, Xu X and Li X 2020 Spatial heterogeneity of climate variation and vegetation response for Arctic and high-elevation regions from 2001–2018 *Environ. Res. Commun.* **2** 011007
Yang L, Guan Q, Lin J, Tian J, Tan Z and Li H 2021 Evolution of NDVI secular trends and responses to climate change: a perspective from nonlinearity and nonstationarity characteristics *Remote Sens. Environ.* **254** 112247
Zhang H K and Roy D P 2016 Landsat 5 Thematic Mapper reflectance and NDVI 27-year time series inconsistencies due to satellite orbit change *Remote Sens. Environ.* **186** 217–33
Zhang Y, Song C, Band L E, Sun G and Li J 2017 Reanalysis of global terrestrial vegetation trends from MODIS products: browning or greening? *Remote Sens. Environ.* **191** 145–55
Zhu Z *et al* 2016 Greening of the Earth and its drivers *Nat. Clim. Change* **6** 791–5
Zhu Z, Wang S and Woodcock C E 2015 Improvement and expansion of the Fmask algorithm: cloud, cloud shadow, and snow detection for Landsats 4–7, 8, and Sentinel 2 images *Remote Sens. Environ.* **159** 269–77
Zhu Z and Woodcock C E 2012 Object-based cloud and cloud shadow detection in Landsat imagery *Remote Sens. Environ.* **118** 83–94
Zivot E and Wang J 2006 *Modeling Financial Time Series with S-PLUS®* (New York: Springer)